Elsevier Editorial System(tm) for
International Journal of Hydrogen Energy
Manuscript Draft

Manuscript Number: HE-D-17-00870

Title: The Role of Gadolinia Doped Ceria Support on the Promotion of CO2 Methanation over Ni and Ni-Fe Catalysts

Article Type: SI: IMPRES2016 (Basile)

Section/Category: Catalysts / Electrocatalysts / Photocatalysts

Keywords: methanation; Gadolinia Doped Ceria; nickel/iron catalyst

Corresponding Author: Dr. Patrizia Frontera, PhD

Corresponding Author's Institution: Università Mediterranea di Reggio Calabria

First Author: Patrizia Frontera, PhD

Order of Authors: Patrizia Frontera, PhD; Anastasia Macario, Professor; Giuseppe Monforte, Researcher; Giuseppe Bonura, Researcher; Marco Ferraro, Researcher; Antonino S Aricò, Researcher; Pierluigi Antonucci, Professor

Abstract: In the present work, CO2 methanation was investigated over Ni, Fe, Ni3Fe1, Ni1Fe1 and Ni1Fe3 catalysts supported on Gadolinia Doped Ceria (GDC) in the temperature range 200-400 °C. Both CO2 and H2 conversion decreased in the order Ni/GDC > Ni3Fe1/GDC > Ni1Fe1/GDC > Ni1Fe3/GDC. No catalytic activity was displayed by Fe/GDC. Maximum CO2 conversion (>90%) was observed at 400° C, with almost 100% selectivity to CH4. The catalysts were characterized by X Ray Diffraction (XRD), N2 adsorption/desorption, H2 - Temperature Programmed Reduction (H2-TPR), Transmission Electron Microscopy (TEM), X-ray Photoelectron Spectroscopy (XPS) and CO2 Temperature Programmed Desorption (CO2-TPD). The superior activity of monometallic Ni/GDC with respect to bimetallic Ni-Fe/GDC catalysts was ascribed to the presence of surface oxygen vacancies induced by the GDC support, as well as to the ability of the Ni-GDC to interact with CO2, as suggested by XPS data.

UNIVERSITÀ DEGLI STUDI "MEDITERRANEA" DI REGGIO CALABRIA
DICEAM, Dipartimento di Ingegneria Civile, dell'Energia, dell'Ambiente e dei Materiali

Dear Editor,

I have the pleasure to submit the manuscript "The Role of Gadolinia Doped Ceria Support on the Promotion of CO_2 Methanation over Ni and Ni-Fe Catalysts" for the publication in International Journal of Hydrogen Energy

Waiting to receive your answer, we thank you heartily.

Kindest regards,

(for the Authors)

Patrizia Frontera

****

Ing. Patrizia Frontera, Ricercatore in Scienza e Tecnologia dei Materiali
Dipartimento di Ingegneria Civile, dell'Energia, dell'Ambiente e dei Materiali (DICEAM)
Università "Mediterranea", Loc. Feo di Vito, 89122 Reggio Calabria, Italy
Phone: +39 0965 875308, Fax: +39 0965 875248; E-mail: patrizia.frontera@unirc.it

The Role of Gadolinia Doped Ceria Support on the Promotion of CO_2 Methanation over Ni and Ni-Fe Catalysts

P. Frontera[a,d]*, A. Macario[b], G. Monforte[c], G. Bonura[c], M. Ferraro[c], A.,S. Aricò[c], P.L. Antonucci[a,d]

[a]Department of Civil, Energy, Environment and Material Engineering, Mediterranean University of Reggio Calabria, Salita Melissari, 89124 Reggio Calabria, Italy

[b]Department of Mechanical, Energy and Management Engineering, University of Calabria, Via P. Bucci 87036, Arcavacata di Rende, Cosenza, Italy

[c]CNR, Institute of Advanced Technologies for Energy "Nicola Giordano" – ITAE, Salita S. Lucia sopra Contesse, 5, 98126 Messina, Italy

[d]INSTM, Consorzio Interuniversitario Nazionale per la Scienza e Tecnologia dei Materiali, Via G. Giusti, 9 - 50121 Firenze, Italy

* Corresponding Author: patrizia.frontera@unirc.it (P. Frontera)

Suggested Reviews

1) Marta Boaro

University of Udine, Italia

Associate Professor, expert in the catalyst field

Email: marta.boaro@uniud.it

2) Dharmendra Pandey

Birla Institute of Technology, Mesra Ranchi, Jharkhand 835215, India

Heterogeneous Catalysis, Reaction Engineering, Environmental Pollution Control, Molecular Dynamics

Email: dpandey.iitk@gmail.com

3) José Luis García Fierro

Profesor de Investigación

Dirección Postal

INSTITUTO DE CATÁLISIS Y PETROLEOQUÍMICA,(CSIC)

c/ Marie Curie, 2 Cantoblanco 28049 Madrid España

Email: jlgfierroicp.csic.es

The Role of Gadolinia Doped Ceria Support on the Promotion of CO_2 Methanation over Ni and Ni-Fe Catalysts

P. Frontera[a,d]*, A. Macario[b], G. Monforte[c], G. Bonura[c], M. Ferraro[c], A.,S. Aricò[c], P.L. Antonucci[a,d]

[a]Department of Civil, Energy, Environment and Material Engineering, Mediterranean University of Reggio Calabria, Salita Melissari, 89124 Reggio Calabria, Italy

[b]Department of Mechanical, Energy and Management Engineering, University of Calabria, Via P. Bucci 87036, Arcavacata di Rende, Cosenza, Italy

[c]CNR, Institute of Advanced Technologies for Energy "Nicola Giordano" – ITAE, Salita S. Lucia sopra Contesse, 5, 98126 Messina, Italy

[d]INSTM, Consorzio Interuniversitario Nazionale per la Scienza e Tecnologia dei Materiali, Via G. Giusti, 9 - 50121 Firenze, Italy

* Corresponding Author: patrizia.frontera@unirc.it (P. Frontera)

Highlight

- The role of Gadolinia doped Ceria support of bimetallic catalyst Ni/Fe have been investigated
- The obtained results showed a superior catalytic activity of the monometallic catalyst whit respect to the bi-metallic ones
- The support play a decisive role in the metal-support interaction.

The Role of Gadolinia Doped Ceria Support on the Promotion of CO_2 Methanation over Ni and Ni-Fe Catalysts

P. Frontera[a,d]*, A. Macario[b], G. Monforte[c], G. Bonura[c], M. Ferraro[c], A.,S. Aricò[c], P.L. Antonucci[a,d]

[a]Department of Civil, Energy, Environment and Material Engineering, Mediterranean University of Reggio Calabria, Salita Melissari, 89124 Reggio Calabria, Italy

[b]Department of Mechanical, Energy and Management Engineering, University of Calabria, Via P. Bucci 87036, Arcavacata di Rende, Cosenza, Italy

[c]CNR, Institute of Advanced Technologies for Energy "Nicola Giordano" – ITAE, Salita S. Lucia sopra Contesse, 5, 98126 Messina, Italy

[d]INSTM, Consorzio Interuniversitario Nazionale per la Scienza e Tecnologia dei Materiali, Via G. Giusti, 9 - 50121 Firenze, Italy

* Corresponding Author: patrizia.frontera@unirc.it (P. Frontera)

ABSTRACT

In the present work, CO_2 methanation was investigated over Ni, Fe, Ni_3Fe_1, Ni_1Fe_1 and Ni_1Fe_3 catalysts supported on Gadolinia Doped Ceria (GDC) in the temperature range 200-400 °C. Both CO_2 and H_2 conversion decreased in the order Ni/GDC > Ni_3Fe_1/GDC > Ni_1Fe_1/GDC > Ni_1Fe_3/GDC. No catalytic activity was displayed by Fe/GDC. Maximum CO_2 conversion (>90%) was observed at 400° C, with almost 100% selectivity to CH_4. The catalysts were characterized by X Ray Diffraction (XRD), N_2 adsorption/desorption, H_2 – Temperature Programmed Reduction (H_2-TPR), Transmission Electron Microscopy (TEM), X-ray Photoelectron Spectroscopy (XPS) and CO_2 Temperature Programmed Desorption (CO_2-TPD). The superior activity of monometallic Ni/GDC with respect to bimetallic Ni-Fe/GDC catalysts was ascribed to the presence of surface oxygen vacancies induced by the GDC support, as well as to the ability of the Ni-GDC to interact with CO_2, as suggested by XPS data.

Keywords: methanation, Gadolinia Doped Ceria, nickel/iron catalyst,

1. Introduction

CO_2 fixation for the synthesis of chemicals has great potential interest as this process can contribute to the reduction of CO_2 emissions in the atmosphere. Being an abundant and renewable carbon source, CO_2 represents an advantageous primary source for sustainable processes involving low GHG emissions.

Amongst viable catalytic processes, CO_2 methanation (Sabatier reaction) [1] is one of the most preferred because of its favourable thermodynamics: $CO_2 + 4\ H_2 = CH_4 + H_2O$ ($\Delta G° = -114$ kJ/mole). Moreover, if hydrogen produced by renewable energy sources is employed, such a process would be able to solve the problems connected with the storage and transportation of hydrogen. In other words, methane would become the preferential hydrogen carrier due to its appropriate storage properties (for example, as liquefied natural gas, LNG) and transportation options in the existing infrastructures [2 -3].

CO_2 methanation has been widely investigated in the past years on several catalytic systems based on noble metals (e.g., Ru, Rh) [3, 4, 10, 11, 13, 14] although most of the studies concerns with oxide-supported Ni [5 – 7, 9, 12], because of its lower cost.

As for noble metals, Ru has been reported to be the most active and stable methanation catalyst, the reaction selectivity depending on the support [8]. In ref. [13], turnover frequencies of the reaction were shown to decrease in the order $Ru/Al_2O_3 > Ru/MgAl_2O_4 > Ru/MgO > Ru/C$, suggesting that the catalytic performance was significantly affected by metal-support interactions. Also the preparation method of the catalyst plays a decisive role on the catalytic activity; exemplarily, Ru/TiO_2 prepared by a barrel-sputtering technique was able to achieve a 100% yield at only 433K, that is much higher in comparison with wet impregnation [14].

Also Al_2O_3-supported Rh was reported to be very active and selective to methane [15], and insights on the reaction mechanism have been recently given [16].

Because of the property of Pd in dissociating molecular hydrogen, a bifunctional $Pd\text{-}Mg/SiO_2$ was investigated for CO_2 methanation, which demonstrated high selectivity (>95%) towards methane, with 59% CO_2 conversion [17]. Also Pt, supported on high surface area titania nanotubes, showed good activity in the reaction carried out at low temperature (100°C) [18].

For what concerns Ni-based systems, main approaches in attempting to discover efficient catalysts have included investigations related to the influence of i) the nature of the support, ii) the preparation method and iii) the design of a suitable catalyst surface constituted by a combination of more than one metal.

Both nature of the support and preparation method play a decisive role in the metal-support interaction, therefore influencing the dispersion and the overall catalytic performance in terms of activity and selectivity. Alumina and amorphous silica-supported Ni were the most extensively investigated catalysts, prepared by different techniques (ion exchange, deposition-precipitation, impregnation) [19-24]. Also ZrO_2 and $Ce\text{-}ZrO_2$-supported Ni have shown very high CO_2 conversion and selectivity to CH_4 [7, 25, 26].

A novel class of methanation catalysts was recently discovered starting from calculations using density functional theory (DFT). According to refs. [27-29], the two important properties of a metal surface in determining the rate of the methanation reaction are the energy barrier for CO dissociation and the stability of the main intermediates on the surface, atomic C and O. DFT calculations of these parameters for different metal surfaces have shown to be linearly correlated in the so-called Bronsted-Evans-Polanyi relation, leading to a volcano-shaped dependence of the rate on the dissociation energy of adsorbed CO. For a weak adsorption, the energy barrier for dissociation is high, thus decreasing the reaction rate. On the other hand, strong adsorption leads to low rates of removal of adsorbed C and O from the surface to form reaction products, as shown in ref. [27].

According to this analysis, Ni_3Fe and NiFe should be good candidates for catalysts having higher activity than the single metals and close to the best ones, Ru and Co. Successive investigations have experimentally proven that NiFe alloys, supported on $MgAl_2O_4$ and Al_2O_3, have significantly higher activity and selectivity to methane in comparison with monometallic Ni and Fe catalysts for both CO and CO_2 hydrogenation [30, 31]. A more recent study has substantially confirmed previous evidences, showing that $Ni_{0.7}Fe_{0.3}/Al_2O_3$ catalyst achieved high carbon dioxide conversion and CH_4 selectivity [32].

The number of papers dealing with the catalytic CO_2 hydrogenation to CH_4 has dramatically increased in the last decade [33]. Nevertheless, no definitive understanding of reaction mechanism has been reached, this goal being necessary for a rational design of a high performance catalyst [34].

On the other hand, utilization of CO_2 as a renewable and environmental friendly source of carbon represents a very attractive approach in view of the use as chemical storage of the excess of electrical energy produced by renewables [35]. In this process, hydrogen used to reduce CO_2 can be preferably produced by electrolysis supplied by renewable energy, making sustainable the entire process.

In order to find new metal-support combinations able to achieve high CH_4 yields, in the present paper results of CO_2 methanation on Gadolinia Doped Ceria (GDC)-supported Ni-Fe catalysts are presented. The choice of such a support is made on the basis of previous studies [36,37] that have demonstrated the "self de-coking" capability of GDC, i.e. removal of carbon species via gasification promoted by the oxygen supplied through the oxide support.

2. Experimental

2.1 Catalysts preparation

Catalysts were prepared by wet impregnation. Two different impregnation procedures were carried out. $Ni(NO_3)_2*6H_2O$ and $Fe(NO_3)_3*9H_2O$ were used as metal precursors. The support was Gadolinia 0.2 Doped Ceria 0.8 (GDC). The precursors were simultaneously solubilized in aqueous ethanol solution (50 %) and then impregnated onto the support at room temperature for 6 hours. Then, the catalysts were dried at T=100°C for 8 hours and calcined at T=600°C for 4 hours to form the metal oxides that are reduced successively. Five catalysts were prepared in all (monometallic Ni/GDC and Fe/GDC, Ni_3Fe_1/GDC, Ni1Fe1/GDC, Ni1Fe3/GDC). The total metal loading was 50%wt deposited onto 50% wt GDC.

2.2 Catalysts characterization

X ray diffraction (XRD) patterns of the powders were recorded on a Bruker D2 Phaser using Cu Kα radiation at 30 kV and 20 mA. Peaks attribution was made according COD Crystallography Open Database.

Samples were characterized by N_2 adsorption/desorption isotherms obtained at the temperature of liquid nitrogen using an automated physisorption instrument (Micromeritics ASAP 2020 analyzer). The samples were evacuated at 300 °C for 1 h prior to the measurements. Total surface area was calculated according to the BET method.

Hydrogen Temperature Programmed Reduction (H_2-TPR) measurements were performed in a fixed-bed reactor at atmospheric pressure, with 50 mg sample loaded in the middle of the reactor tube. The reduction gas was 5% H_2/Ar at a total flow rate of 50 ml/min. The system was heated at a rate of 10°C/min up to 800°C. The H_2 uptake during the reduction was analyzed on line by a gas chromatograph with a thermal conductivity detector (TCD).

The Transmission Electron Microscopy (TEM) analysis was carried out using a Jeol 2010 F instrument operated at 120 kV, able to achieve a 0.19 nm point-to-point resolution and a 0.14 nm line resolution.

Carbon deposited during reaction was evaluated by using a CHNS-O Flash EA ^{TM} 1108 THERMO FINNIGAN elementary analysis instrument. Few milligrams of used catalysts were encapsulated and treated at high temperature in air. CO_2 produced during oxidation process was analysed by a high sensitivity TC detector.

X-ray photoelectron microscopy (XPS) data were collected on a PHI 5800 spectrometer with a monochromatic Al source. The charging effects were corrected by adjusting the binding energy of

C1s peak from adventitious carbon to 284.6 eV. The characterization experiments were carried out for fresh (before reaction) and spent (after reaction) samples.

The CO_2-TPD study on the GDC support was carried out using a linear quartz microreactor (id = 4 mm, l = 200 mm) according to [38]. 220.7 mg of the support was reduced at 800°C for 4 hrs with H_2. After 4 hrs the H_2 stream was replaced by Ar for 0.5 hr at 800°C. Then, the sample was cooled to 250°C, afterwards CO_2 was supplied instead of Ar and cooled again to 210°C for 0.5 hr. The CO_2 stream was replaced by Ar, heating the sample up to 500°C at a ramp rate of 5°C/min, maintaining the sample at this temperature for 0.5 hr. The CO_2-TPD profile was integrated and the number of moles of desorbed CO_2 was determined by pulse calibration of known amounts of CO_2 in Ar.

2.3 Catalytic tests

The catalytic experiments were carried out under atmospheric pressure using a continuous fixed-bed microreactor having an inner diameter of 6 mm. Gas inlet streams, purified by Chrompack filters, were measured by Brooks 5850S flow-meters. The temperature of all micro-plant compartments was controlled by heating belts consisting in electric resistances, measured by thermocouples connected to thermoregulators to keep constant the temperature at 145°C. The catalytic performance experiments were conducted in the temperature range 200-400°C at 30,000 h^{-1} gas hourly space velocity (GHSV). Effluent gases from the reactor were analyzed, after removal of water from the exit stream, through condensation and silica gel trap, by two Varian CP4900 chromatographs with a thermal conductivity detector (TCD) and fitted with three columns (MS5A, Porapak Q and CPsil), using He as carrier gas for the analysis of CH_4, CO, CO_2, O_2, C_2H_4, N_2 and N_2 to detect H_2.

CO_2 and H_2 conversion were defined as follows:

χ_{CO2}= $moles_{CO2}$ in – $moles_{CO2}$ out / $moles_{CO2}$ in

χ_{H2}= $moles_{H2}$ in – $moles_{H2}$ out / $moles_{H2}$ in

Selectivity is defined as follows:

S_{CH4}= $moles_{CH4}$ produced / $moles_{CO2}$ converted

3. Results and discussion

3.1 Physico-chemical characterisation

Table 1 reports the total surface area of the catalysts and of the GDC support.

The results show that the BET surface area of the catalysts decreases significantly by metal addition, likely due to the formation of large Ni and Fe oxide aggregates, which limits the access to the internal surface of the support.

However, no trend was observed when the Ni and Fe composition on the support was changed. Previous studies on supported Ni–Fe catalysts preparation also showed a surface area decrease with the increase of the metal content and no specific trend with the change in Ni and Fe composition was observed [31,38].

XRD patterns of the fresh catalysts prepared by co-impregnation and reduced in 5% H_2/Ar at 550°C are shown in Fig. 1. The pattern (a) referred to monometallic Ni/GDC catalyst, clearly shows the fcc cubic structure of Ni. The cubic structure of gadolinia-doped ceria is also clearly evident. The main peaks of Ni, e.g. the (111) reflection, are slightly shifted to higher Bragg angles in the Ni/GDC sample compared to bulk Ni reported in the literature. This is possibly due to the dispersion of nanosized Ni particles on gadolinia-doped ceria. The Ni_3Fe_1/GDC and Ni_1Fe_1/GDC patterns (b and c, respectively) appear quite similar. The (111) reflection of the cubic structure of Ni is shifted to lower Bragg angles in the Ni_3Fe_1/GDC, revealing the possible occurrence of a Ni-Fe alloy. The shift to lower Bragg angles also occurs, but at a larger extent, in the Ni_1Fe_3 (pattern d) sample, according to the literature. These evidences are in line with the formation of a Ni-Fe alloy in accordance to the Vergards' law. Yet, a smaller shift was recorded for the Ni-Fe sample indicating lower extent of alloy formation in this sample. Moreover, the Ni_3Fe_1 sample showed some mixed Ni-Fe phases.

In the pattern (e) related to Fe/GDC, all peaks appear to be related to Fe_3O_4, suggesting that almost no reduction of the oxide occurred after the hydrogen treatment in this specific sample.

The reducibility of the mono- and bimetallic catalysts, after calcination, was investigated by H_2-TPR. Fig. 2 shows the H_2-TPR profiles of Ni/GDC (a), Ni_3Fe_1/GDC (b), Ni_1Fe_1/GDC (c), Ni_1Fe_3/GDC (d) and Fe/GDC (e). It can be seen that the presence of a second metal modifies the reduction profiles of the mono-metallic catalysts, as expected. The reduction pattern of Ni/GDC reveals the presence of two peaks centered at about 396 ° and 426 °C due to the reduction of bulk NiO and of NiO species that have interacted more strongly with the support, respectively [38]. The reduction profile of Fe/GDC (e) shows three broad peaks at about 407°, 604° and 754 °C, attributable to the progressive reduction of Fe_2O_3 (or Fe_3O_4 where this phase is occurring). The profile of Ni_1Fe_3 resembles that of Fe/GDC, with two broad peaks at about 627° and 770 °C, still related to the reduction of Fe_2O_3. The Ni_1Fe_1 and Ni_3Fe_1 catalysts show well defined peaks at about 420°C, almost corresponding to the reduction temperature of NiO. A broad shoulder at about 704 °C is visible in the Ni_1Fe_1 profile, probably due to the reduction of Fe_2O_3. The appearance of a

single peak in the TPR profile, showing the simultaneous reduction of two metal oxides, is likely indicative of alloy formation in the bimetallic catalysts [39]. On this basis, the TPR profiles shown in Fig. 2 suggest that the Ni and Fe species are likely alloyed on the catalysts surface of Ni_1Fe_1 and Ni_3Fe_1 samples. Such evidences appear to be in accordance with the XRD results of Ni_3Fe_1/GDC and Ni_1Fe_1/GDC catalysts. As to the Ni_1Fe_3 sample, no appearance of alloying is envisaged from the observation of the TPR profile. Moreover, a surface enrichment phenomenon could have been occurred; in the present case Fe, having a higher surface energy with respect to Ni [40], inclines to migrate towards the surface of the catalyst; as a result, a different composition between bulk and surface occurs. Furthermore, XPS results [41,42] appear to confirm such an hypothesis (see below).

The XPS spectra of Ni2p core level in the fresh and used monometallic Ni/GDC are shown in Fig. 3a. The fresh catalyst shows the occurrence of a broad peak at about 855 eV which can be attributed to both Ni_2O_3 and $Ni(OH)_2$, since these species are characterised by very similar binding energies.

The used catalyst shows essentially the occurrence of metallic Ni and Ni oxides (lower B.E. photoelectron bands). The Ni oxide species with paramagnetic structure give rise to satellite peaks at 860.7 eV and 873 eV, whereas the usual satellite at the about 879 eV is overlapping with the onset of the Ce oxide band, and thus it is not reported here. Ni oxides are prevailing, with a main peak due to the convolution of Ni_2O_3 and $Ni(OH)_2$ (855.5 eV) showing a shoulder at lower B.E. attributed to NiO (853.5 eV), whereas metallic Ni occurs at about 852 eV.

The adsorption of CO_2 species on the catalyst surface is clearly observed from the increase of the carboxylic functional group (288.9 eV) in the C1s spectrum upon operation (Fig. 3b).

The formation of adsorbed CO_2 species can be also clearly observed from the O1s spectrum (Fig. 3 c). Interestingly, from the O1s pattern one can compare the oxygen peak related to the metal oxide with the peak associated to the adsorbed CO_2 which occurs at higher B.E. (531.4 eV). The peak associated to the metal oxide is prevailing in the fresh sample (529 eV), whereas there is a strong increase of the signal associated to the adsorbed CO_2 in the used sample (531.4 eV) revealing an excellent capability of the catalyst to chemisorb CO_2 during the catalytic reaction.

In Fig. 4a, related to the Ni2p spectrum of the Ni_3Fe_1/GDC catalyst, the well defined peak at 855.2 eV could denote the presence of NiO and $Ni(OH)_2$, although a contribution of NiOOH can be also taken into account. This considering that the signal of the latter species appears at 855.75 eV, thus making undistinguishable the relative contribution of these species; also the presence of some Ni_2O_3 cannot be ruled out. In the spectrum (Fig. 4a), the signal of metallic Ni is also visible at 852.6 eV. The Ni2p signal in the used Ni_3Fe_1 catalyst is characterized by a larger content of Ni^{2+} species i.e. NiO and $Ni(OH)_2$ than the Ni_1Fe_1 catalyst (see below). The Fe2p spectrum (Fig. 4b) indicates the prevailing presence of Fe_2O_3 (711.64 eV), together with that of Fe in its metallic form at 706.64 eV.

The O1s spectrum (Fig. 4c) shows a lower B.E. peaks associated to the presence of Ni, Fe and Ce oxides (529.13 eV), which are not easily distinguished, whereas adsorbed CO_2 occurs at 531.6 eV. The Ni/Fe atomic ratio is considerably lower than that expected (1.12).

Fig. 5a shows the Ni2p core level spectrum of the Ni_1Fe_1/GDC catalyst. Main signals appear at at about 856 and at 852 eV, attributed to Ni_2O_3 and to metallic Ni, respectively. The presence of Ni^{2+} in its hydroxide form and/or NiOOH (about 855 eV), this latter corroborated by the signal at 861.3 eV attributable to the satellite peak of Ni oxide species, is envisaged. The main Ni2p signal of the fresh catalyst is broader than that of the used catalyst and slightly shifted to higher B.E. values. This indicates a larger occurrence of Ni oxide species with higher oxidation state in the fresh catalyst. In Fig. 5b the spectrum related to Fe2p core level is reported. The signal at 711.61 eV, related to Fe_2O_3, is predominant, whereas a weak signal attributable to metallic Fe is visible at 707 eV. The Fe 2p spectra show characteristics similar to the Ni 2p. In the fresh catalyst, the main Fe 2p peak appears broader and shifted to higher B.E. compared with that of the used catalyst. It is derived that, also in this case, the fresh catalyst is composed by a larger number of oxidized Fe species than the used catalyst. Such aspects are in accordance to the reducing conditions (H_2) occurring during reaction. These are in part mitigated by the large excess of CO_2 (oxidizing species) and formation of water, according to the Sabatier reaction. Thus, the Ni_1Fe_1 catalyst, discharged under the same reaction environment, shows a prevailing occurrence of low valence state oxides of Ni_1Fe_1 species on the surface with lower evidence of metallic Ni and Fe species.

These results are not in disagreement with XRD since the catalysts were first reduced at 600°C in pure H_2 and thereafter exposed to the reaction environment at lower temperatures (200-400°C). The surface properties evidenced in the XPS results are more affected by the reaction environment than the bulk properties (XRD), which are essentially determined by the initial reduction process. It is noteworthy that the Ni/Fe atomic concentration is 0.72, denoting a surface enrichment in Fe, as above hypothesized.

The lower occurrence of oxide species in the used catalysts appears to be strengthened by the examination of the O1s spectrum, where the peak of the metal oxides is clearly visible at 529.6 eV. This peak increases in the used sample compared to the fresh one. The peak at about 532 eV is attributable to the presence of adsorbed CO_2 (Fig.5c).

Also for the fresh Ni_1Fe_3 sample, the Ni^{2+} is largely occurring as $Ni(OH)_2$ and Ni_2O_3 with a small shoulder attributable to NiO (Fig. 6a). In Fig. 6a, it is also clearly distinguishable the peak of metallic Ni (852.5 eV). There are clear evidences that, by significantly increasing the Fe content in the catalyst (Ni_1Fe_3), a larger fraction of low valence state Ni species occurs in the fresh sample. This denotes the occurrence of a charge transfer between Fe and Ni, being Ni more electronegative.

The Fe2p spectrum (Fig. 6b) again confirms Fe_2O_3 as predominant species (about 711 eV), with a very little contribution of metallic Fe, denoted by the signal at 706 eV (Fig. 6b). A reduced signal of Ni and Fe hydroxides appears in the O1s spectrum at 531.6 eV. The peak at 529.5 eV is related to the adsorbed CO_2 species (Fig. 6c). For this sample, the experimental Ni/Fe atomic ratio is 0.20, denoting a strong enrichment of iron on the surface.

As above evidenced, the used $NiFe_3$ sample shows similar features for the Fe2p signal to the pristine sample, however there is almost no more evidence of the small peak associated to metallic Fe (Fig. 6b) and, more surprisingly, no relevant amount of Ni is observed on the surface (Fig. 6a). This evidence means that there is an alloy occurring for the Fe-Ni system with strong enrichment of Fe on the outermost layers (Fe skin layer) upon operation in the methanation reaction. The catalytic activity decreases accordingly.

The CO_2 adsorption of the Fe-enriched catalyst, as observed from the analysis of the C1s and O1s photoelectron lines, appears much less strong compared to the pure Ni catalyst (see Fig. 3b-c and Fig. 6 c-d). In Fig. 6d (Ni_1Fe_3), the C1s signal shows a peak associated to the presence of carbonylic species both in the fresh and used samples. The peak at 288.5 eV appears more evident in the used sample. Interestingly, the O1s line in the used sample at 531.5 eV does not reveal the expected increase of the peak related to the adsorbed CO_2 as in the case of the Ni/GDC sample discussed above (Fig. 3 b,c); in fact, this signal remains much lower than that of the metallic oxide peak in Fig. 6c (Ni_1Fe_3). Moreover, the ratio between the oxygen linked to metallic oxide and that deriving from the adsorbed CO_2 is larger in the used sample than in the fresh catalyst (Fig. 6c).

It is clearly observed that the O1s peak associated to the adsorbed CO_2 (~531 eV) in the used samples (Figs. 3-6) decreases progressively in relative intensity, compared to the oxygen signal associated to the transition metal oxides (~529 eV), with the decrease of Ni content in the catalyst. This is related to the effect of the different surface chemistry that affects the propensity of interaction with carbon dioxide. This would indicate that there is a scavenging effect for the adsorbed CO_2 played by Fe species on the surface, especially when Ni is present at low content in the outermost layers, as indicated in Fig. 6a (used sample).

Such effect corroborates the fact that the sample rich in Fe is less prompt to adsorb CO_2 than Ni rich catalysts and would thus result in a lower catalytic activity (see below).

GDC support did not undergo any transformation during the tests for all catalytic formulations.

TEM analysis was carried out on the mono-metallic Ni/GDC catalyst and on bimetallic Ni_3Fe_1/GDC, Ni_1Fe_1/GDC and Ni_1Fe_3/GDC catalysts, both fresh and used. The micrograph of the fresh Ni/GDC catalyst (Fig. 7a) shows Ni particles homogeneously distributed onto the support, with dimensions in the range 3-8 nm. GDC particles are in the range 200-400 nm. In the spent

sample, no relevant sintering of Ni particles is apparent; some migration from the bulk to the surface seems to occur for Ni particles on the GDC support. Some reduction of the size of GDC particles is envisaged. The Ni_3Fe_1 fresh sample (Fig. 8a) shows a morphology characterized by GDC particles sized 200-400 nm and small Ni-Fe oxides distributed on the surface of the support. Also in this case, some reduction in size of GDC is observed after reaction, but the Ni-Fe particles are not much affected by operation (Fig. 8b). No carbon is visible from the examination of the micrographs. The micrograph of the Ni_1Fe_1/GDC sample (Fig. 9a) exhibits support particles ranging from 100 to 400 nm in size, surrounded by clusters of Ni-Fe oxides containing metal particles sized 5-15 nm. After reaction (Fig. 9b), a significant reduction in dimension of the GDC particles is observed (up to 50 nm about), and the Ni oxide particles do not change significantly in size (see image at high magnification).

A more compact morphology can be observed for the Ni_1Fe_3 catalyst. The GDC size ranges between 400 and 600 nm, while the Ni-Fe oxides appear not well dispersed (Fig. 10a). After reaction (Fig. 10b), the GDC particles are much smaller and almost spherical in shape. In the high magnification image the Ni-Fe species are clearly visible. For this catalyst, some amorphous (polymer-type) carbon is observed.

As discussed above, for all formulations the size of GDC particles was reduced during operation. This could indicate that, during the reaction, the water formed causes some disruption of the larger GDC particles and, at the same time, exerts an oxidizing action on the metal particles, avoiding complete reduction. No carbon deposition is observed on the surface of the used catalysts. In this respect, the role of the GDC support is decisive in terms of oxygen vacancies, providing lattice defects, which improve the oxygen mobility and inhibit carbon deposition [43-45].

Anyhow, the possible presence of carbon on all the spent bimetallic catalysts was investigated with a CHNS analyzer. Carbon contents of 0.428, 0.817 and 1.008 % wt./wt. were detected for Ni_3Fe_1, Ni_1Fe_1 and Ni_1Fe_3, respectively. This could be amorphous carbon not easily identified by TEM analysis; however, the amount is low and could not influence significantly the reaction process.

3.2 Catalytic studies

The reaction conditions adopted in the experiments were: H_2/CO_2 molar ratio = 4; GHSV = 30,000 h^{-1}; atmospheric pressure; T = 200, 300, 400°C. The catalytic activity (conversion of CO_2 and H_2) of all samples is reported in Fig. 11 (dry basis). The water produced was separated from the reaction system by a water-cooled condenser. The selectivity to CH_4 was almost 100% in all experiments; no by-products were detected by the gas analysis system. Conversion increased as temperature

increased (Fig. 11). Both CO_2 and H_2 conversion decreased in the order Ni/GDC > Ni_3Fe_1/GDC > Ni_1Fe_1/GDC > Ni_1Fe_3/GDC. No catalytic activity was displayed by Fe/GDC.

Contrary to the premises based on DFT calculations mentioned in the Introduction, the monometallic Ni/GDC catalyst exhibited a superior performance with respect to the bimetallic systems, in particular Ni_3Fe_1 and Ni_1Fe_1, under the experimental conditions of the present work. It has been previously underlined the pivotal role of the support in determining the activity of the catalyst in the CO_2 methanation reaction [34], through its influence on the dimension of the active metal particles, reducibility of the catalyst and nature of active sites. It is worth mentioning that most of the previous studies on Ni and/or Ni-Fe catalysts for CO_2 methanation have dealt with SiO_2, Al_2O_3, ZrO_2, TiO_2, CaO-Al_2O_3 and Mg-Al spinel as supports [31, 38, 46].

On the other hand, the promotion action of ceria on Ni catalysts supported on Al_2O_3 and carbon nanotubes has been recently reported [47-49]. In particular, the promoting action of ceria on Ni/Al_2O_3 catalyst was explained by Ramani et al. [47] by an increase of dispersion of metal Ni on the support and a positive modification of the electronic structure of Ni caused by a strong interaction between Ni and Ce. In the reducing environment of the reaction, Ce_2O_3 and CeO_2 may co-exist, generating oxygen vacancies in the structure that release electrons migrating from ceria through Ni-CeO_2 interface and, in this way, increasing the electron density of Ni. Thus, the addition of CeO_2 to Ni produced a weakening of the C=O bond of CO_2 adsorbed on Ni active sites and increased the dissociation, with subsequent hydrogenation of CO_2 [50]. It is noteworthy that the positive role played by the presence of oxygen vacancies also applies to supports different from ceria (ZrO_2, $Ce_{0.5}Zr_{0.5}O_2$ in particular [51-54]).

Furthermore, the superior performance of ceria-supported Ni catalysts determined by reduction of CO_2 molecules by active Ni species and by the presence of surface oxygen vacancies, thus promoting CO_2 methanation, supports furthermore the evidence that both factors concur to the high catalytic activity of monometallic Ni catalyst. Therefore, on the basis of previous literature and of the present experimental results, it can be envisaged that the predicted superior catalytic activity of bimetallic Ni-Fe systems with respect to monometallic Ni can be associated only to the presence of supports that are not characterised by proper oxygen mobility. For supports with low oxygen mobility, FeOx could play a role similar to CeO_2 in producing oxygen vacancy sites.

Pandey and Deo [38] reported that incomplete reduction of iron oxides occurred on TiO_2, SiO_2 and Nb_2O_5; therefore, for these systems there is a limited availability of metallic Ni and Fe to form the alloy.

The ability of Al_2O_3 to adsorb CO_2 was thought to be responsible for the maximum relative enhancement observed for the Ni-Fe/Al_2O_3 catalyst. Moreover, the authors reported a CO_2

adsorption value of 838 μmol CO_2/g Al_2O_3. Our CO_2-TPD experiments (Fig. 12), carried out according to the procedure reported in ref. [38], showed a relatively high CO_2 uptake of 741μmol CO_2/g GDC. Since CO_2 adsorbs on basic sites, the basicity of the support seems to play a decisive role towards the activity of the catalyst for the reaction. Martin and Duprez [55] reported the following scale for the density of basic sites of some metal oxides: CeO_2 > MgO > ZrO_2 > Al_2O_3 > SiO_2. Furthermore, rare earth oxides (such as Gd_2O_3) are known to enhance the surface basicity of pure CeO_2 [56]. These evidences confirm the paramount role of GDC in promoting the reaction process and thus the superfluous role of Fe in the bimetallic catalyst when ceria is present as support and acts as co-catalyst.

Conclusions

In the present paper, a series of bi-metallic Ni-Fe catalysts supported on GDC, as well as mono-metallic Ni/GDC and Fe/GDC catalysts, were synthesized and characterized for the CO_2 methanation reaction. The obtained results showed a superior catalytic activity of the mono-metallic Ni/GDC catalyst with respect to the bi-metallic ones. On the basis of previous literature and of the present results, it is envisaged that the predicted superior catalytic activity of bi-metallic Ni-Fe systems with respect to mono-metallic Ni can be associated only to the presence of supports that do not evidence proper oxygen mobility. In this respect, it is evident the pivotal role of the GDC support in generating surface oxygen vacancies able to weaken the carbon-oxygen bond of CO_2 adsorbed on Ni sites and to increase the dissociation, with subsequent CO_2 hydrogenation.

Acknowledgements

The Authors gratefully acknowledge the financial support from the Italian Ministry of Economic Development (MiSE) through the project "Accordo di Programma Ricerca di Sistema – CNR, Sistemi elettrochimici per la generazione e l'accumulo di energia".

References

[1] Sabatier P, Senderens JB. Direct Hydrogenation of Oxides of Carbon in Presence of Various Finely Divided Metals. Compt Rend 1902;134:689-691.

[2] Meylan FD, Morean V, Elkman S. Material constraints related to storage of future European renewable electricity surpluses with CO_2 methanation. Energy Pol 2016; 94:366-376.

[3] Beuls A, Swalus C, Jacquemin M, Heyen G, Karelovic A, Ruiz P. Methanation of CO_2: Further insight into the mechanism over Rh/γ-Al_2O_3 catalyst. Appl Catal B: Environ 2012; 113–114: 2–10.

[4] Weatherbee GD, Bartholomew CH. Hydrogenation of CO_2 on group VIII metals. J Catal 1981; 68: 67-76.

[5] Yamasaki M, Habazaki H, Asami K, Izumiya K, Hashimoto K. Effect of tetragonal ZrO on the catalytic activity of Ni/ZrO catalyst prepared from amorphous Ni-Zr alloys. Catal Commun 2006; 7: 24-28.

[6] Aksoylu AE, IlsenOlsan Z. Hydrogenation of carbon oxides using coprecipitated and impregnated Ni/Al2O3 catalysts. Appl Catal A Gen 1997; 164: 1-11.

[7] Ocampo F, Louis B, Roger AC. Methanation of carbon dioxide over nickel-based Ce0.72Zr0.28 O_2 mixed oxide catalysts prepared by sol-gel method. Appl Catal A Gen 2009; 369: 90-96.

[8] Frontera P, Macario A, Ferraro M, Antonucci P. Supported Catalysts for CO_2 Methanation: A Review. Catal 2017;7:59-87

[9] Trovarelli A. Catalytic properties of Ceria and CeO_2- containing materials. Catal Rev Sci Eng 1996; 38: 439-520.

[10] de Leitenburg C, Trovarelli A, Kaspar J, A Temperature-Programmed and Transient Kinetic Study of CO_2 Activation and Methanation over CeO_2 Supported Noble Metals. J Catal 1997;166: 98-107.

[11] Trovarelli A, de Leitenburg C, Dolcetti G, Llorca J. CO_2 Methanation Under Transient and Steady-State Conditions over Rh/CeO_2 and CeO_2-Promoted Rh/SiO_2: The Role of Surface and Bulk Ceria. J Catal 1995; 151: 111-124.

[12] Trovarelli A, de Leitenburg C, Boaro M, Dolcetti G. The utilization of ceria in industrial catalysis. Catal Today 1999; 50: 353-367.

[13] Kowalczyk Z, Stolecki K, Rarog-Pilecka W, Miskiewicz E, Wilczkowska E. Supported ruthenium catalysts for selective methanation of carbon oxides at very low COx/H_2 ratios. Appl Catal A General 2008; 342: 35-39.

[14] Abe T, Tanizawa M, Watanabe K, Taguchi A. CO_2 methanation property of Ru nanoparticle-loaded TiO_2 prepared by a polygonal barrel-sputtering method. Energy Environ Sci 2009; 2(3): 315-321.

[15] Ruiz P, Jacquemin M, Blangenois N. Patent WO 2010006386;2010.

[16] Jacquemin M, Beuls A, Ruiz P. Catalytic production of methane from CO_2 and H_2 at low temperature: Insight on the reaction mechanism. Catal Today 2010; 157: 462-466.

[17] Park JN, McFarland EW. A highly dispersed Pd–Mg/SiO_2 catalyst active for methanation of CO_2. J Catal 2009; 266: 92-97.

[18] Yu KP, Yu WY, Kuo MC, Liou YC, Chien SH. Pt/titania-nanotube: A potential catalyst for CO_2 adsorption and hydrogenation. Appl Catal B Environmental 2008; 84: 112-118.

[19] Chang FW, Kuo MS, Tsay MT, Hsieh MC. Hydrogenation of CO_2 over nickel catalysts on rice husk ash-alumina prepared by incipient wetness impregnation. Appl Catal A General 2003; 247(2): 309-320.

[20] Chang FW, Hsiao TJ, Chung SW, Lo JJ. Nickel supported on rice husk ash—activity and selectivity in CO_2 methanation. Appl Catal A General 1997; 164(1-2): 225-236.

[21] Chang FW, Hsiao TJ, Shih JD, Hydrogenation of CO_2 over a rice husk ash supported nickel catalyst prepared by deposition- precipitation. Ind Eng Chem Res 1998; 37(10):3838-3845.

[22] Chang FW, Tsay MT, Liang SP. Hydrogenation of CO_2 over nickel catalysts supported on rice husk ash prepared by ion exchange. Appl Catal A General 2001; 209(1-2): 217-227.

[23] Chang FW, Tsay MT, Kuo MS. Effect of thermal treatments on catalyst reducibility and activity in nickel supported on RHA-Al_2O_3 systems. Thermochimica Acta 2002; 386(2):161-172.

[24] Puxley DC, Kitchener IJ, Komodromos C, Perkyns N D. In Preparation of Catalysts. Amsterdam; Elsevier; 1983.

[25] Hashimoto K, Habazaki H, Yamasaki M, Meguro S, Sasaki T, Katagiri H, Matsui T, Fujimura K, Izumiya K, Kumagai N, Akiyama E. Advanced materials for global carbon dioxide recycling. Mater Sci Eng A 2001; 304–306: 88-96.

[26] Perkas N, Amirian G, Zhong Z, Teo J, Gofer Y, Gedanken A. Methanation of carbon dioxide on Ni catalysts on mesoporous ZrO2 doped with rare earth oxides. Catal Lett 2009; 130: 455-462.

[27] Bligaard T, Norskov JK, Dahl S, Matthiesen J, Christensen CH, Sehested J. The Bronsted-Evans-Polanyi relation and the volcano curve in heterogeneous catalysis. J Catal 2004; 224: 206-217.

[28] Anderson MP, Bligaard T, Kustov A, Larsen KE, Greeley J, Johannessen T, Christensen CH, Norkov JK. Toward computational screening in heterogeneous catalysus: Pareto-optimal methanation catalysts. J Catal 2006; 239: 501-506.

[29] Norskov JK, Bligaard T, Rossmeisl J, Christensen CH. Towards the computational design of solid catalysts. Nature Chem 2009; 1: 37-46.

[30] Kustov AL, Frey AM, Larsen KE, Johannessen T, Norskov JK, Christensen CH. CO methanation over supported bimetallic Ni-Fe catalysts: From computational studies towards catalyst optimization. Appl Catal A General 2007; 320: 98-104.

[31] Sehested J, Larsen KE, Kustov AL, Frey AM, Johannessn T, Bligaard T, Andersson MP, Norskov JK, Christensen CH. Discovery of technical methanation catalysts based on computational screening. Topics in Catal 2007; 45 (1-4): 9-13.

[32] Kang SH, Ryu JH, Kim JH, Seo SJ, Yoo YD, Sai Prasad PS, Lim HJ, Byun CD. Co-methanation of CO and CO_2 on the Nix-Fe1-x /Al_2O_3 catalysts; effect of Fe contents. Korean J Chem Eng 2011; 28 (12): 2282-2286.

[33] Su X, Xu J, Liang B, Duan H, Hou B, Huang Y. Catalytic carbon dioxide hydrogenation to methane: A review of recent studies. J. Ener Chem 2016; 25(4): 553-565.

[34] Wang W, Gong J. Methanation of carbon dioxide: an overview. Front Chem Sci Eng 2011;5 (1): 2-10.

[35] Centi G, Quadrelli EA, Perathoner. Catalysis for CO_2 conversion: A key technology for rapid introduction of renewable energy in the value chain of chemical industries Energy Environ Sci 2013; 6:1711-1731.

[36] Huang TJ, Yu TC, Effect of steam and carbon dioxide pretreatments on methane decomposition and carbon gasification over doped-ceria supported nickel catalyst. Catal Lett 2005 102 (3):175-181.

[37] Huang TJ, Lin HC, Yu T.C. A Comparison of Oxygen-vacancy Effect on Activity Behaviors of Carbon Dioxide and Steam Reforming of Methane over Supported Nickel Catalysts. Catal. Lett. 2009;105: 239-247.

[38] Pandey D, Deo G. Effect of support on the catalytic activity of supported Ni–Fe catalysts for the CO methanation reaction. J Ind Eng Chem,2016; 33: 99-107.

[39] Bathia S, Belteraminik JN, Do DD. Temperature programmed analysis and its application in catalytic systems. Catal. Today 1990; 7 (3): 309-438.

[40] Vitos L, Ruban AV, Skriver HL, Kollar J, The surface energy of metals. Surf Sci 1998; 411(1): 186-202.

[41] Moulder JF, Stickle WF, Sobol PE, Bomben KD. Handbook of X-ray Photoelectron Spectroscopy 1992, Ed. J. Chastain, R.C. King, Jr., Publ. By Physical Electronics, Inc., Eden Prairie, Minnesota, USA.

[42] Biesinger MC, Payne BP, Grosvenor AP, Lau LWM, Gerson AR, Smart RStC. Resolving surface chemical states in XPS analysis of first row transition metals, oxides and hydroxides: Cr, Mn, Fe, Co and Ni. Appl Surf Sci 2011; 257(7): 2717-2730.

[43] Tada S, Shimizu T, Kameyama H, Haneda T, Kikuchi R. Ni/CeO_2 catalysts with high CO_2 methanation activity and high CH_4 selectivity at low temperatures. Int. J. Hydrogen Energy 2012; 37(7): 5527-5531.

[44] Ocampo F, Louis B, Kiwi-Minsker L, Roger AC. Effect of Ce/Zr composition and noble metal promotion on nickel based $CexZr_1$-xO_2 catalysts for carbon dioxide methanation. Appl Catal A: General 2011; 392: 36-44.

[45] Huang TJ, Wang CH. Methane decomposition and self de-coking over gadolinia doped ceria – supported Ni catalysts. Chem Eng J 2007; 132: 97-103.

[46] Pandey D, Deo G. Promotional effects in alumina and silica supported bimetallic Ni-Fe catalysts during CO_2 hydrogenation. J Mol Catal A: Chem. 2014; 382: 23-30.

[47] Rahmani S, Rezaei M, Meshkani F. Preparation of promoted nickel catalysts supported on nanocrystalline gamma alumina for carbon dioxide methanation. J Ind Eng Chem 2014; 20: 4176-4182.

[48] Liu H, Zou X, Wang X, Lu X, Ding W. Effect of CeO_2 addition on Ni/Al_2O_3 catalysts for methanation of carbon dioxide with hydrogen. J Nat Gas Chem 2012; 21: 703-707.

[49] Wang W, Chu W, Wang N, Yang W, Jiang C. Mesoporous nickel catalyst supported on multi-walled carbon nanotubes for carbon dioxide methanation. Int J Hydrogen Energy 2015; 41 (2): 967-975.

[50] Zhou G, Liu H, Cui K, Jia A, Hu G, Jiao Z, Liu Y, Zhang X. Role of surface Ni and Ce species of Ni/CeO_2 catalyst in CO_2 methanation. Appl Surf Sci 2016; 383: 248-252.

[51] Pan Q, Peng J, Sun T, Gao D, Wang S. CO_2 methanation on Ni/Ce0.5Zr0.5 O_2 catalysts for the production of synthetic natural gas. Fuel Process. Techn. 2014;123:166-171.

[52] Takano H, Shinomija H, Izumija K, Kumagai N, Habazaki H, Hashimoto K, CO_2 methanation of Ni catalysts supported on tetragonal ZrO_2 doped with Ca^{2+} and Ni^{2+} ions. Int. J Hydrogen En 2015; 40:8347-8355.

[53] Takano H, Kirihata Y, Izumija K, Kumagai N, Habazaki H, Hashimoto K, Highly active Ni/Y-doped ZrO_2 catalysts for CO_2 methanation. Appl Surf Sci Part B 2016; 388: 653-663.

[54] Ren J, Qin X, Yang JZ, Qin ZF, Guo HL, Lin JY, Li Z. Methanation of carbon dioxide over Ni-M/ZrO_2 (M = Fe, Co, Cu) catalysts: Effect of addition of a second metal. Fuel Process Techn 2015;137: 204-211.

[55] Martin D, Duprez D. Evaluation of the acid-base surface properties of several oxides and supported metal catalysts by means of model reactions. J. Molecular Catal, A: Chemical 1997; 118: 113-128.

[56] Bernal S, Blanco G, El Amarti A, Fitian L, Galtayries A, Martin J, Pintado JM. Surface basicity of ceria-supported lanthana. Influence of the calcination temperature. Surf Interface Anal 2006; 38: 229-233.

Table 1: Surface area of the samples

Sample	BET area m^2/g
GDC	15.10
50%wt. Ni/GDC	8.76
50%wt. Ni_3Fe/GDC	8.94
50%wt. Ni_1Fe_1/GDC	8.36
50%wt. Ni_1Fe_3/GDC	8.49
50%wt. Fe/GDC	9.02

Captions to figures

Fig. 1 X-ray diffraction of fresh catalyst powders and GDC support with the assignments of the reflections to specific phases.

Fig. 2 Temperature programmed reduction of the fresh catalysts

Fig. 3 High resolution X-ray photoelectron spectroscopy of the Ni/GDC sample before and after operation

Fig. 4 High resolution X-ray photoelectron spectroscopy of the Ni_3Fe_1/GDC sample before and after operation

Fig. 5 High resolution X-ray photoelectron spectroscopy of the Ni_1Fe_1/GDC sample before and after operation

Fig. 6 High resolution X-ray photoelectron spectroscopy of the Ni_1Fe_3/GDC sample before and after operation

Fig. 7 Transmission electron micrographs of the Ni/GDC sample before (a) and after operation (b)

Fig. 8 Transmission electron micrographs of the Ni_3Fe_1/GDC sample before (a) and after operation (b)

Fig. 9 Transmission electron micrographs of the Ni_1Fe_1/GDC sample before (a) and after operation (b)

Fig. 10 Transmission electron micrographs of the Ni_1Fe_3/GDC sample before (a) and after operation (b)

Fig. 11 Variation of catalytic conversion of CO_2 and H_2 as a function of the Ni - Fe contents at different temperatures

Fig. 12 CO_2 desorption rate over the GDC support as a function of temperature

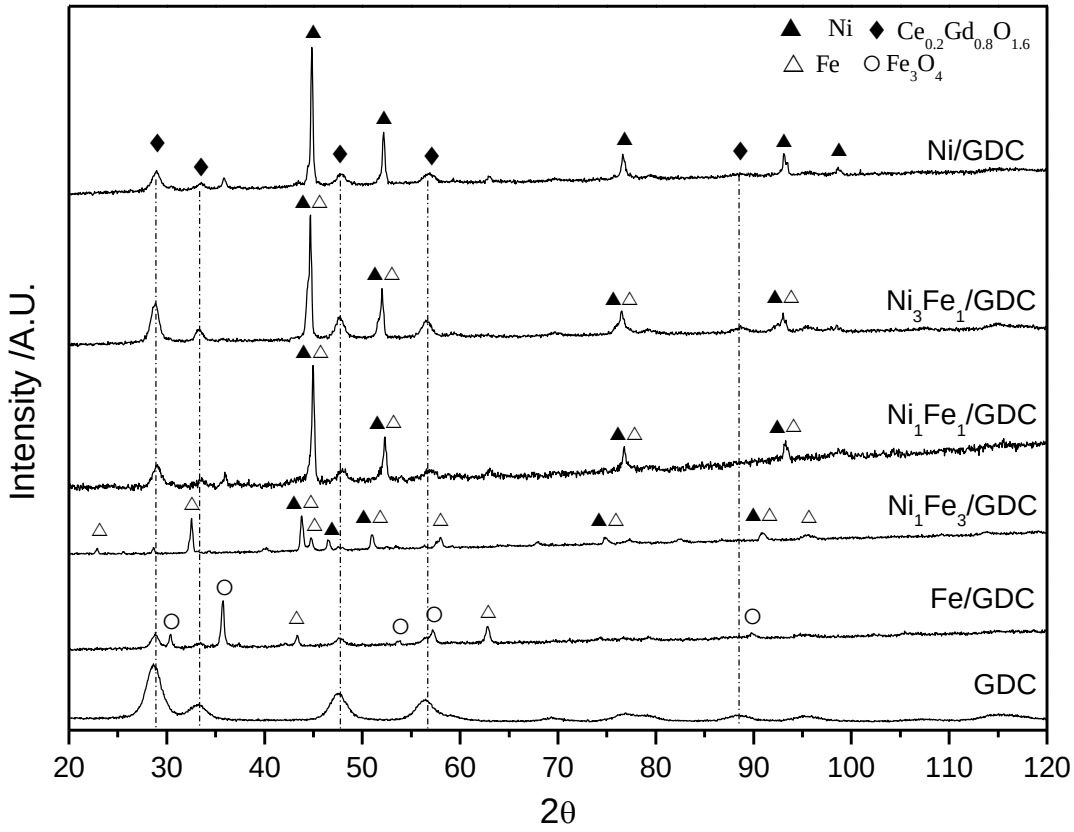
Ni
Ce0.2Gd0.8O1.6
Fe
Fe3O4
Ni/GDC
Ni3Fe1/GDC
Ni1Fe1/GDC
Ni1Fe3/GDC
Fe/GDC
GDC
Intensity /A.U.
20
30
40
50
60
70
80
90
100
110
120
2θ

Figure 1

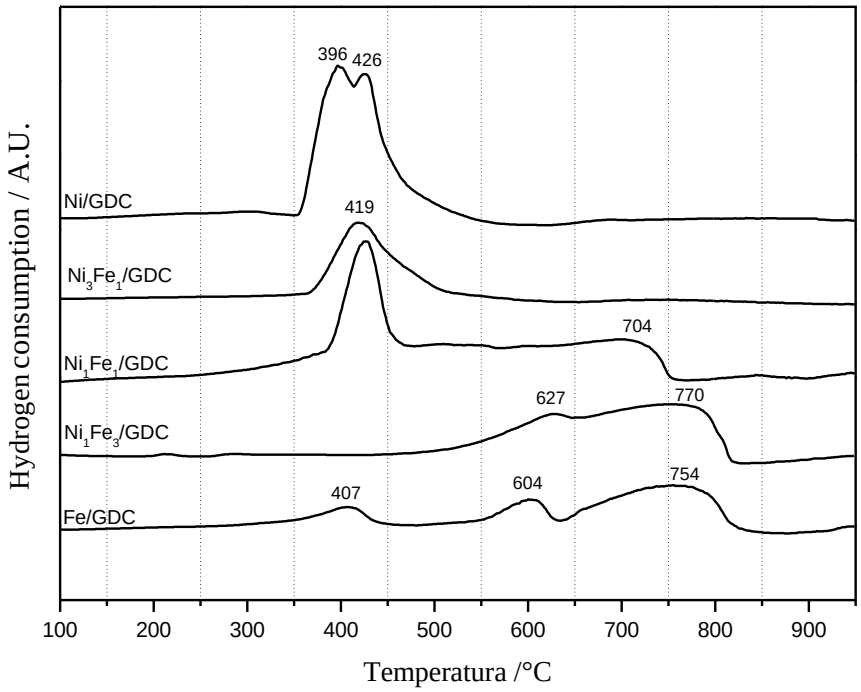
396
426
Ni/GDC
419
Ni3Fe1/GDC
704
Ni1Fe1/GDC
627
770
Ni1Fe3/GDC
407
604
754
Fe/GDC
Hydrogen consumption / A.U.
100
200
300
400
500
600
700
800
900
Temperatura /°C

Figure 2

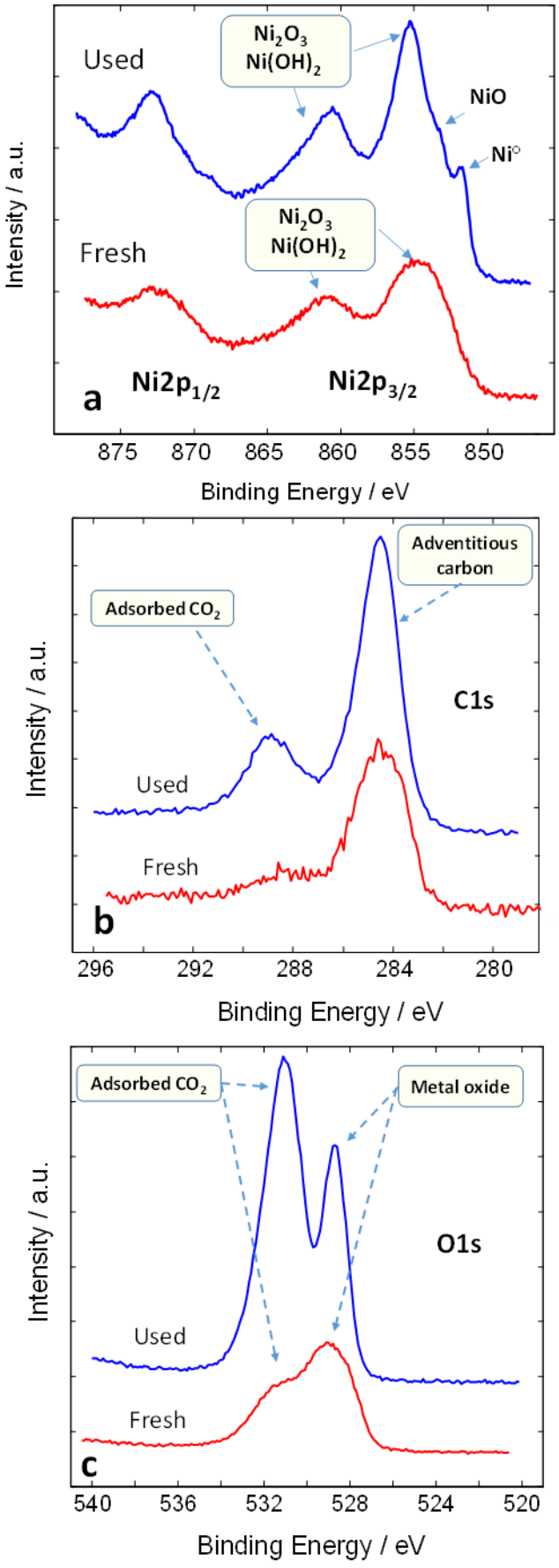
Used
Ni_2O_3
$Ni(OH)_2$
NiO
Ni°
Fresh
Ni_2O_3
$Ni(OH)_2$
a
$Ni2p_{1/2}$
$Ni2p_{3/2}$
Intensity / a.u.
875 870 865 860 855 850
Binding Energy / eV
Adventitious carbon
Adsorbed CO_2
C1s
Used
Fresh
b
Intensity / a.u.
296 292 288 284 280
Binding Energy / eV
Adsorbed CO_2
Metal oxide
O1s
Used
Fresh
c
Intensity / a.u.
540 536 532 528 524 520
Binding Energy / eV

Figure 3

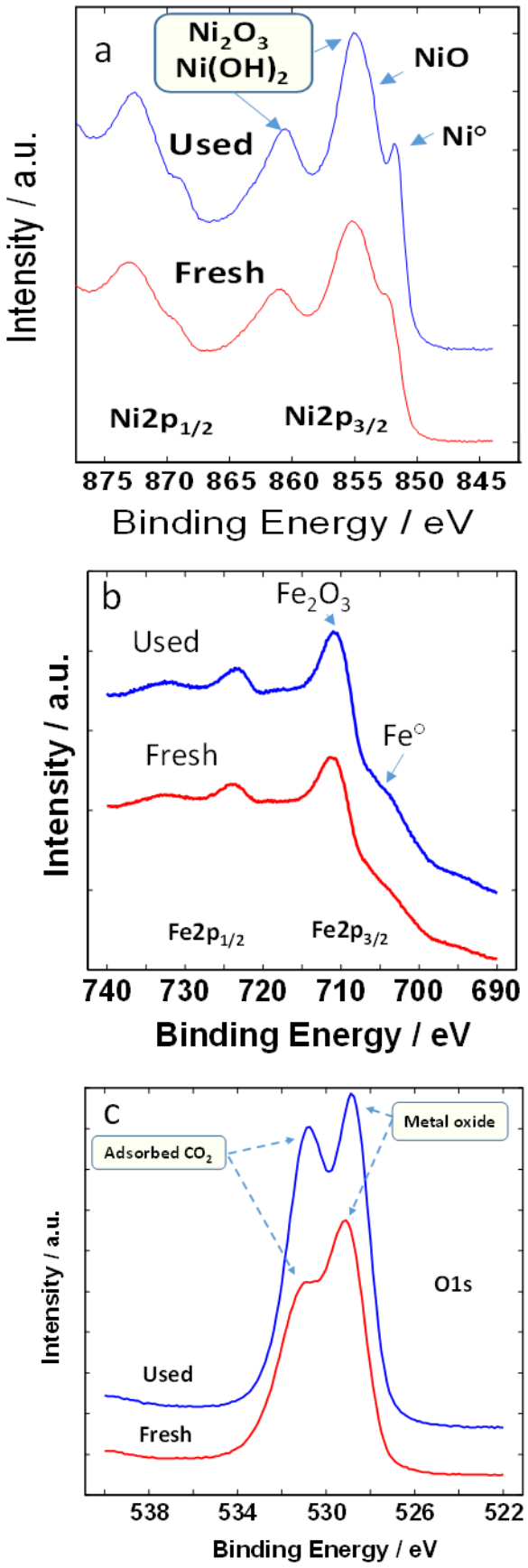
a
Ni_2O_3
$Ni(OH)_2$
NiO
Ni°
Used
Fresh
$Ni2p_{1/2}$
$Ni2p_{3/2}$
Intensity / a.u.
875 870 865 860 855 850 845
Binding Energy / eV
b
Fe_2O_3
Used
Fresh
Fe°
$Fe2p_{1/2}$
$Fe2p_{3/2}$
Intensity / a.u.
740 730 720 710 700 690
Binding Energy / eV
c
Adsorbed CO_2
Metal oxide
O1s
Used
Fresh
Intensity / a.u.
538 534 530 526 522
Binding Energy / eV

Figure 4

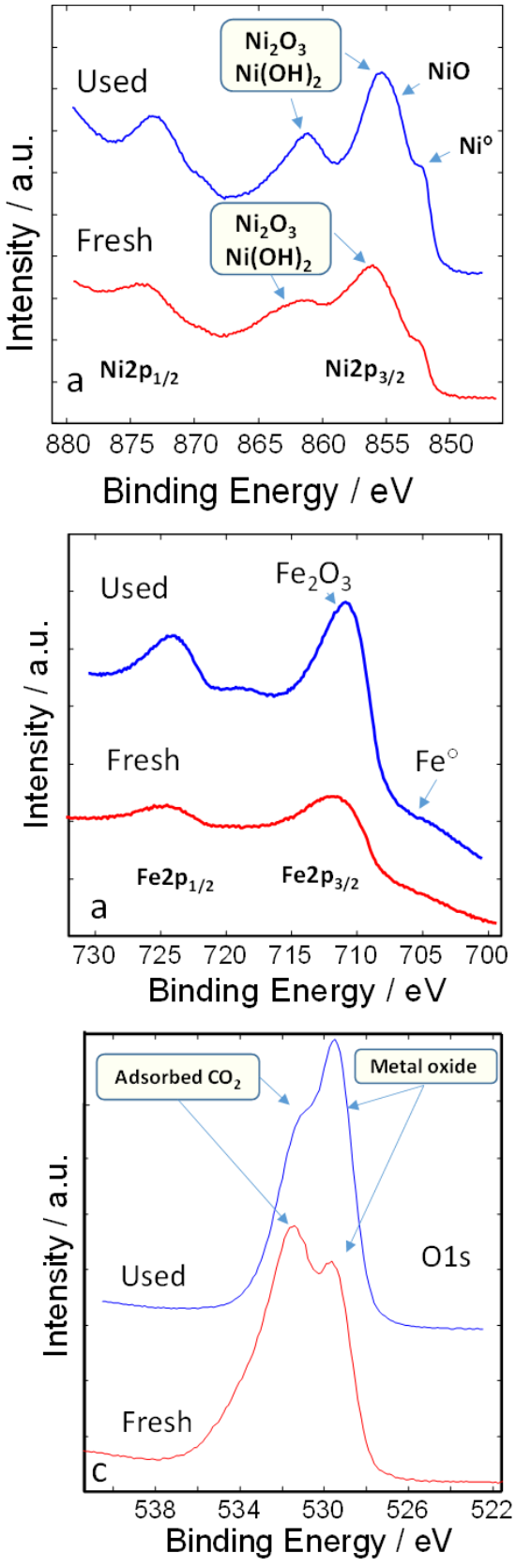
Used
Ni2O3
Ni(OH)2
NiO
Ni°
Fresh
Ni2O3
Ni(OH)2
a
Ni2p1/2
Ni2p3/2
Intensity / a.u.
880 875 870 865 860 855 850
Binding Energy / eV
Used
Fe2O3
Fresh
Fe°
Fe2p1/2
Fe2p3/2
a
Intensity / a.u.
730 725 720 715 710 705 700
Binding Energy / eV
Adsorbed CO2
Metal oxide
Used
O1s
Fresh
c
Intensity / a.u.
538 534 530 526 522
Binding Energy / eV

Figure 5

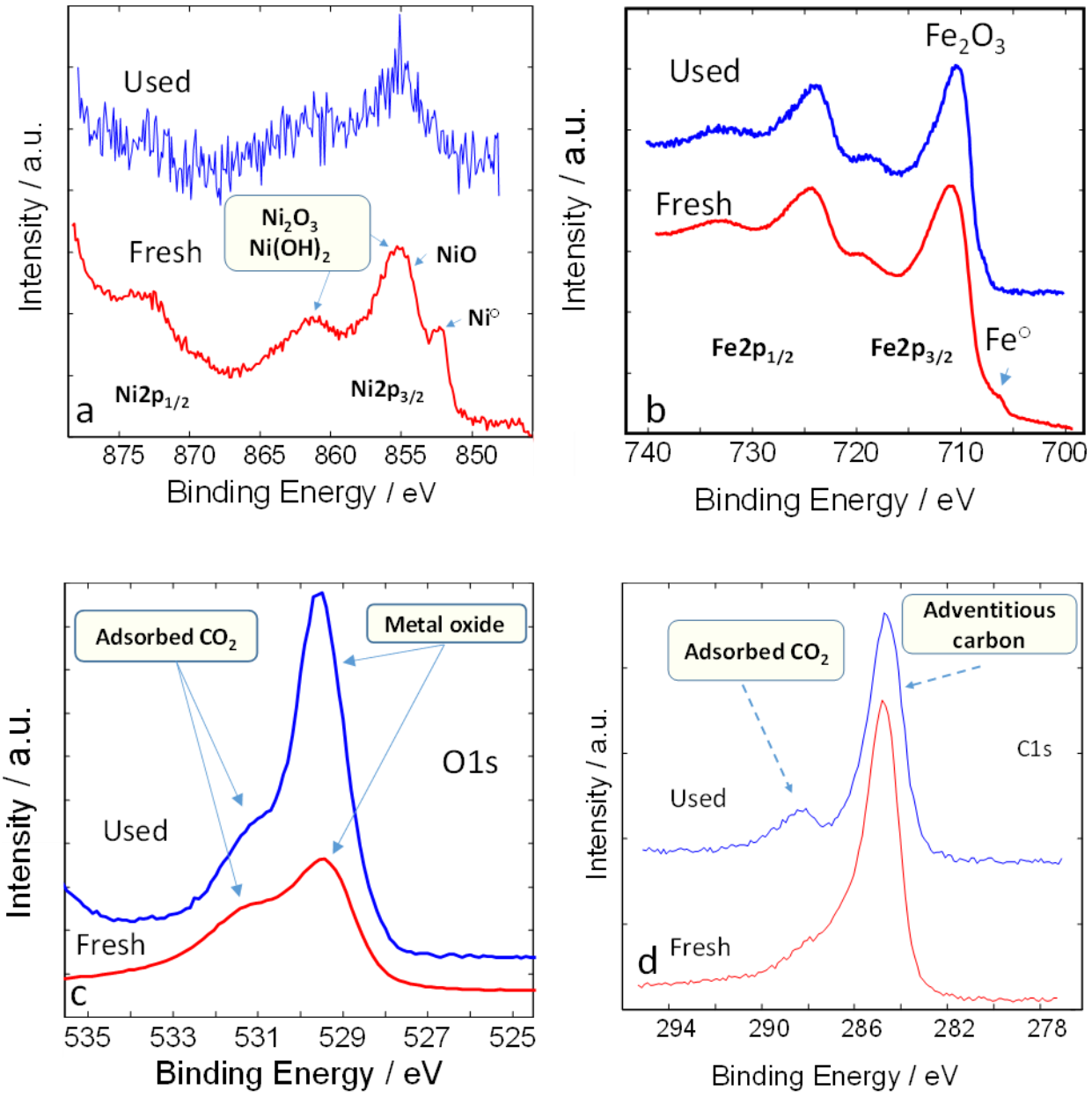
Used
Fresh
Ni2O3
Ni(OH)2
NiO
Ni°
Ni2p1/2
Ni2p3/2
a
Intensity / a.u.
875 870 865 860 855 850
Binding Energy / eV
Fe2O3
Used
Fresh
Fe2p1/2
Fe2p3/2
Fe°
b
740 730 720 710 700
Adsorbed CO2
Metal oxide
O1s
Used
Fresh
c
535 533 531 529 527 525
Adventitious carbon
C1s
d
294 290 286 282 278

Figure 6

a) Ni-GDC fresh

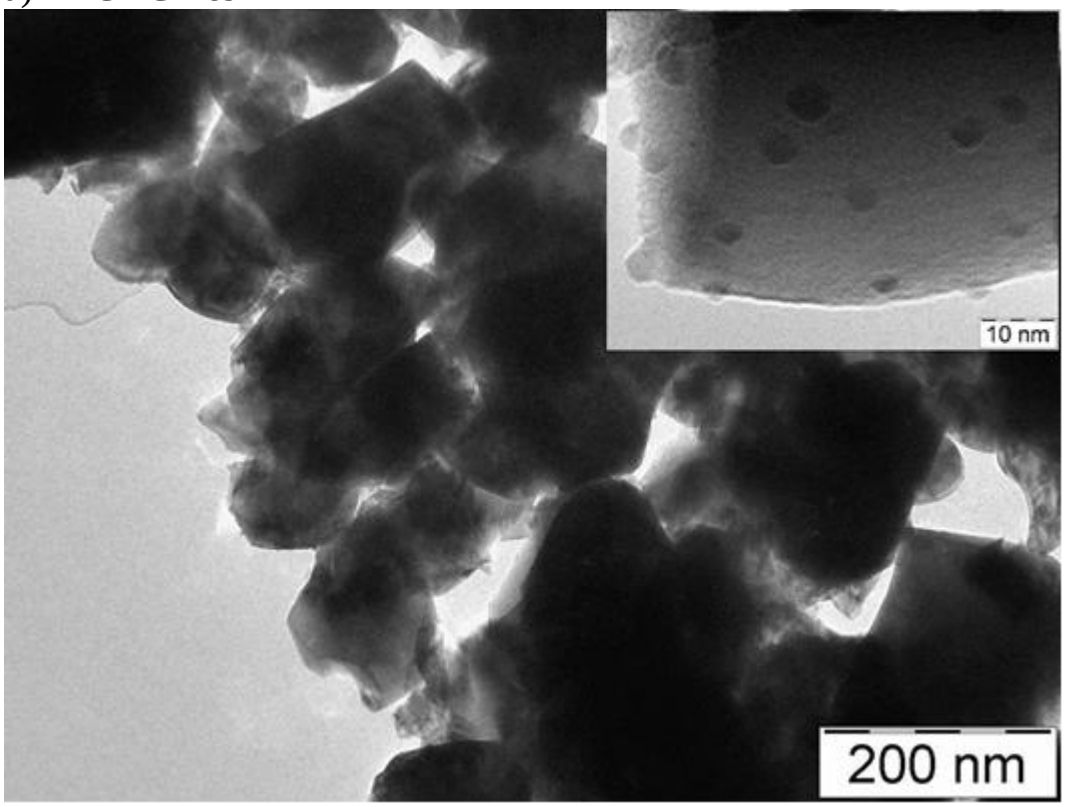

b) Ni-GDC used

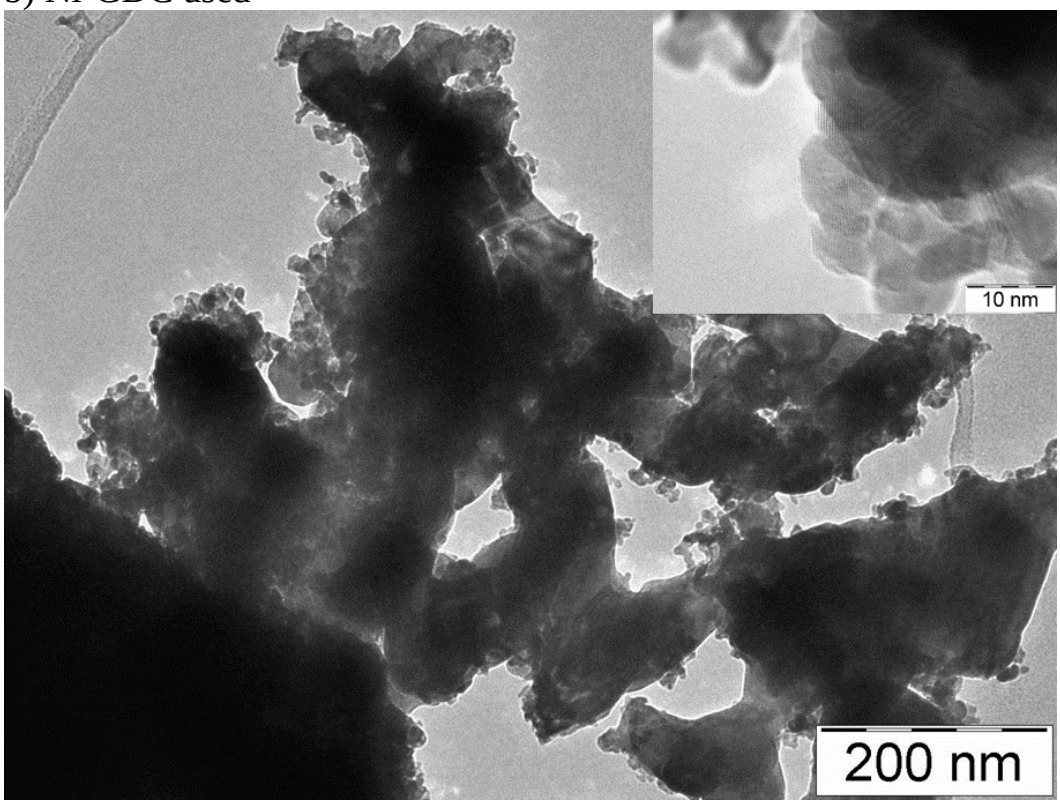

Figure 7

a) Ni_3Fe/GDC fresh

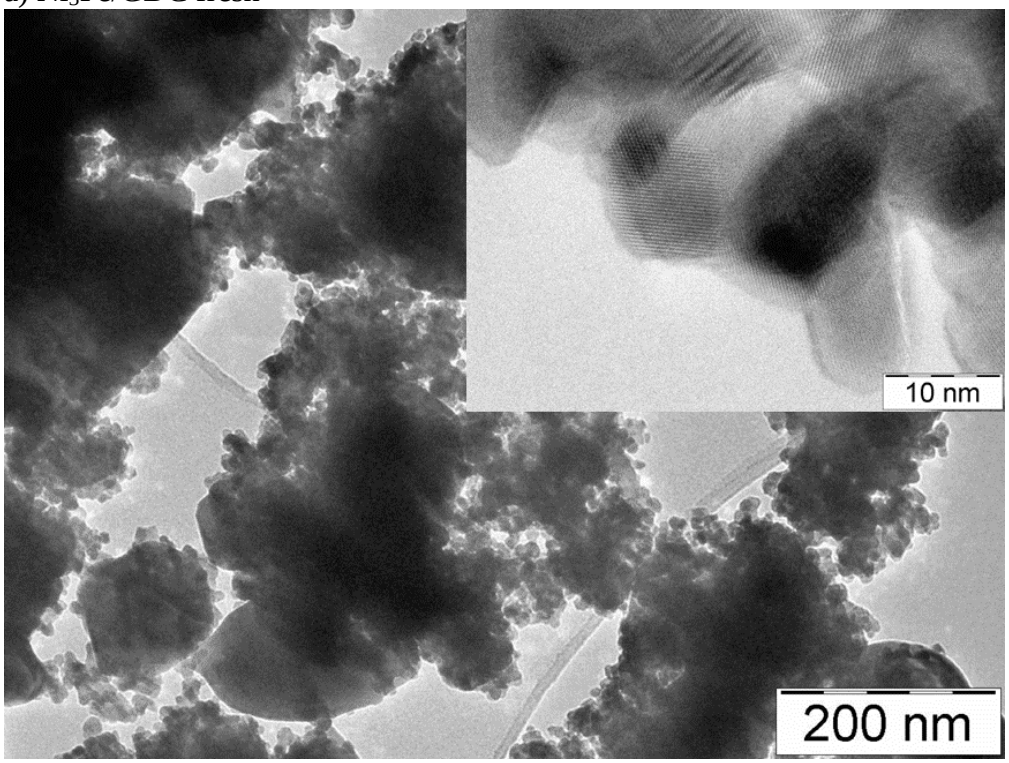

b) Ni_3Fe/GDC used

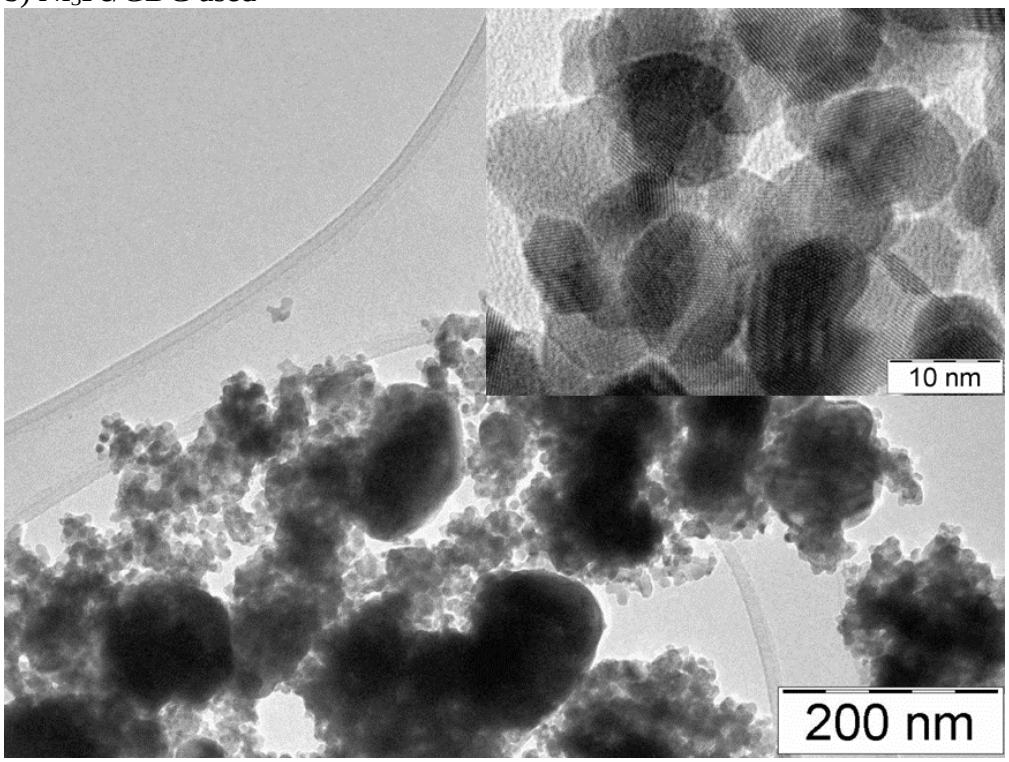

Figure 8

a) NiFe/GDC fresh

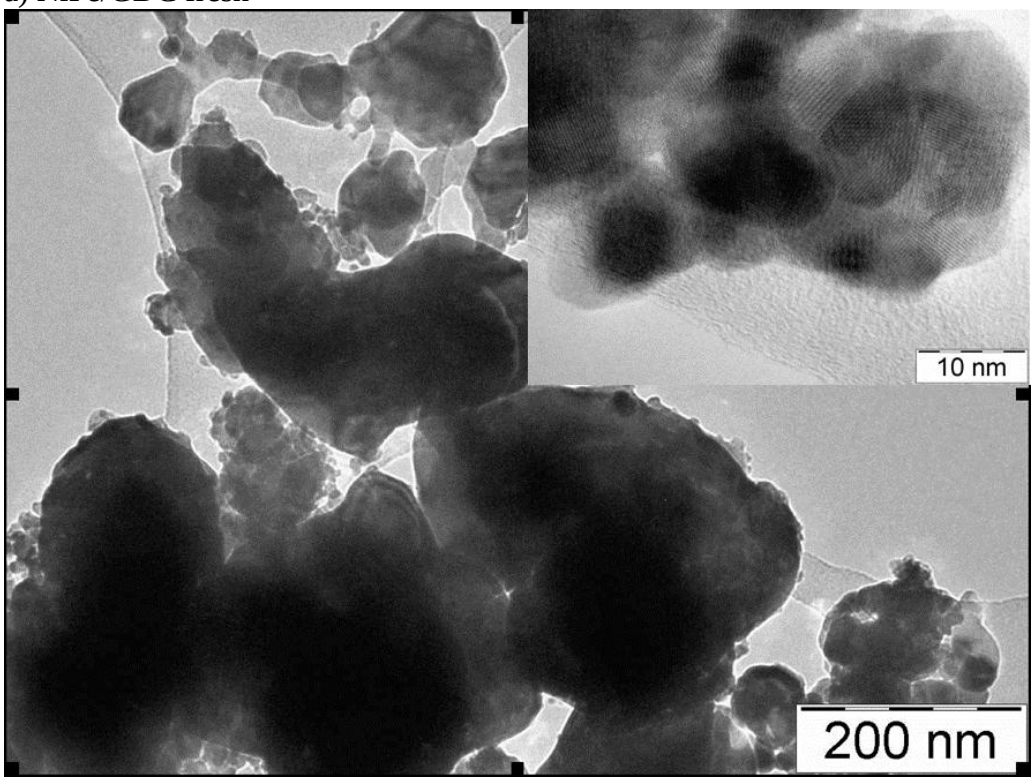

b) NiFe/GDC used

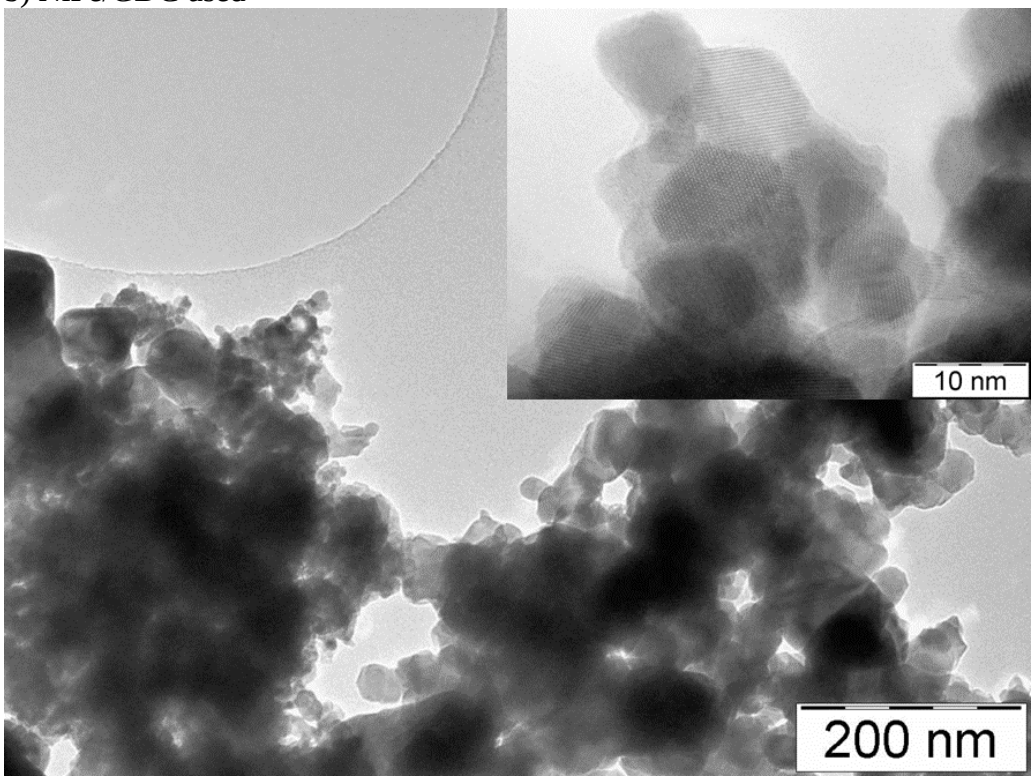

Figure 9

a) $NiFe_3$/GDC fresh

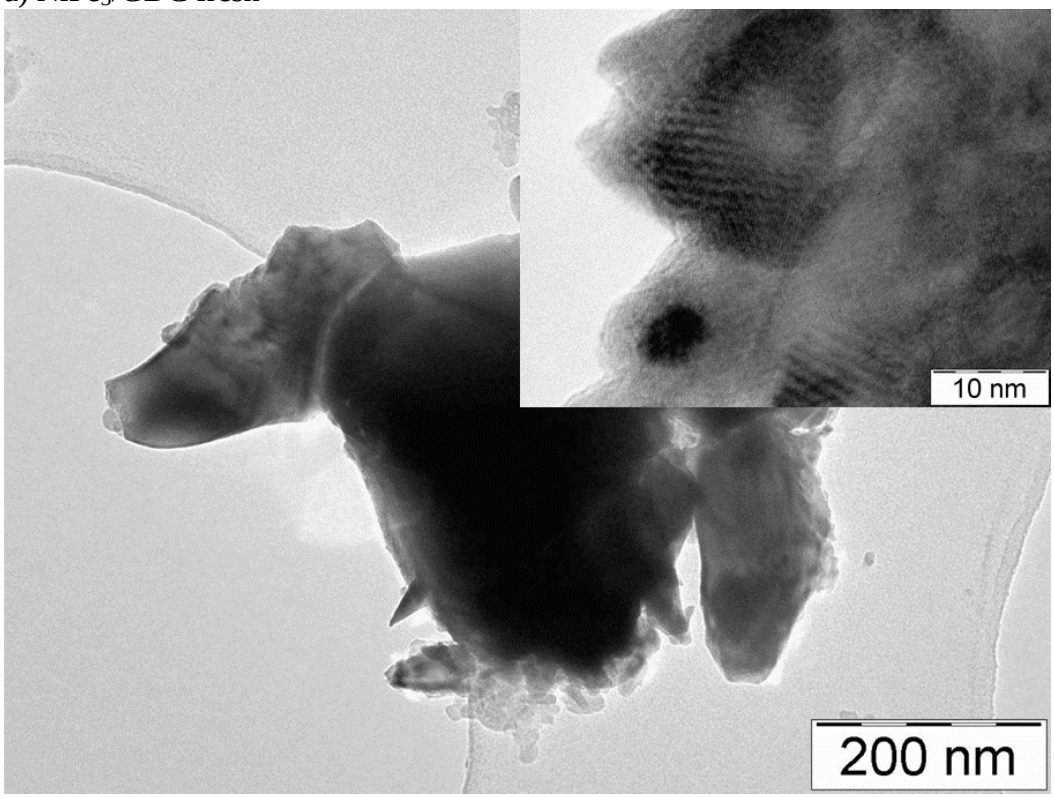

b) $NiFe_3$/GDC used

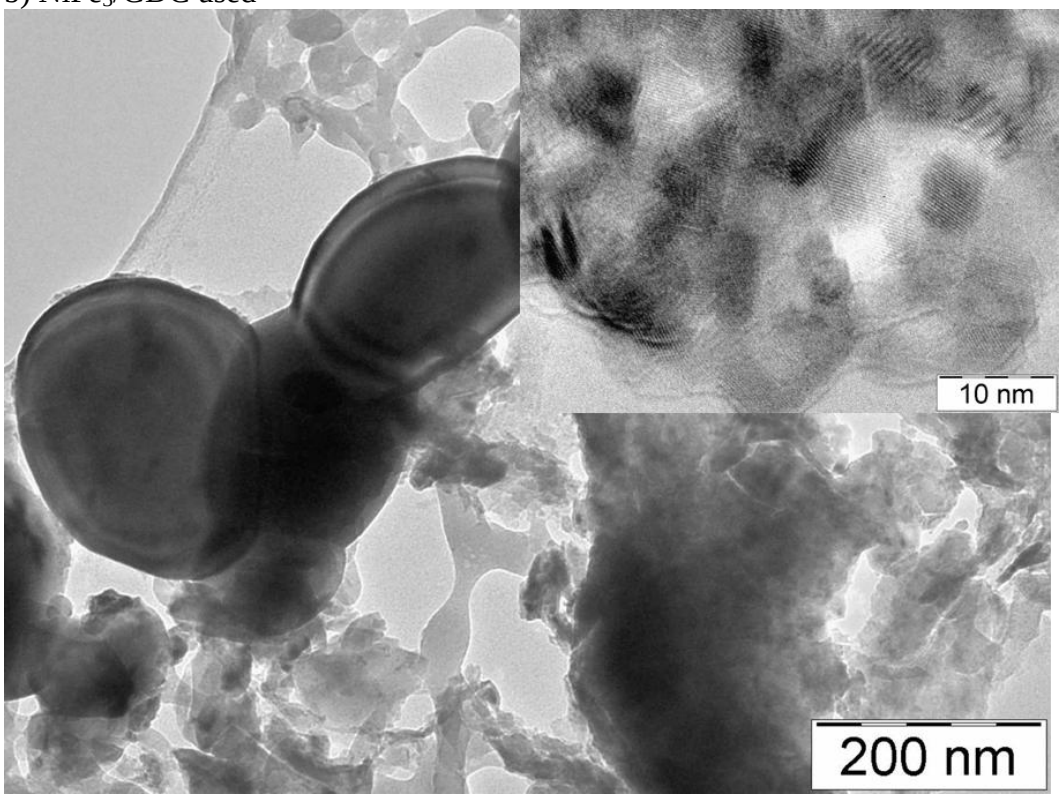

Figura 10

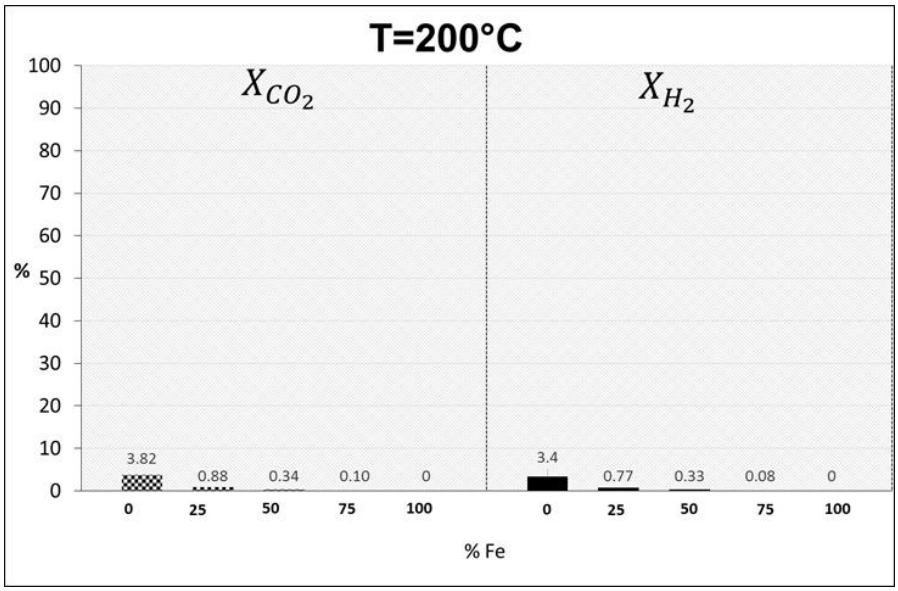
T=200°C
X_{CO_2}
X_{H_2}
%
3.82
0.88
0.34
0.10
0
3.4
0.77
0.33
0.08
0
0
25
50
75
100
% Fe

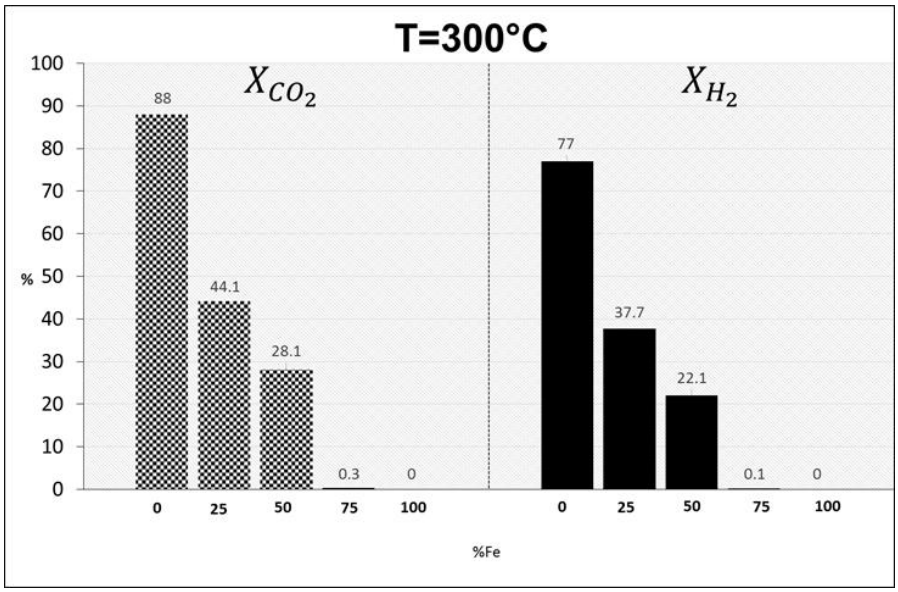
T=300°C
X_{CO_2}
X_{H_2}
%
88
44.1
28.1
0.3
0
77
37.7
22.1
0.1
0
0
25
50
75
100
%Fe

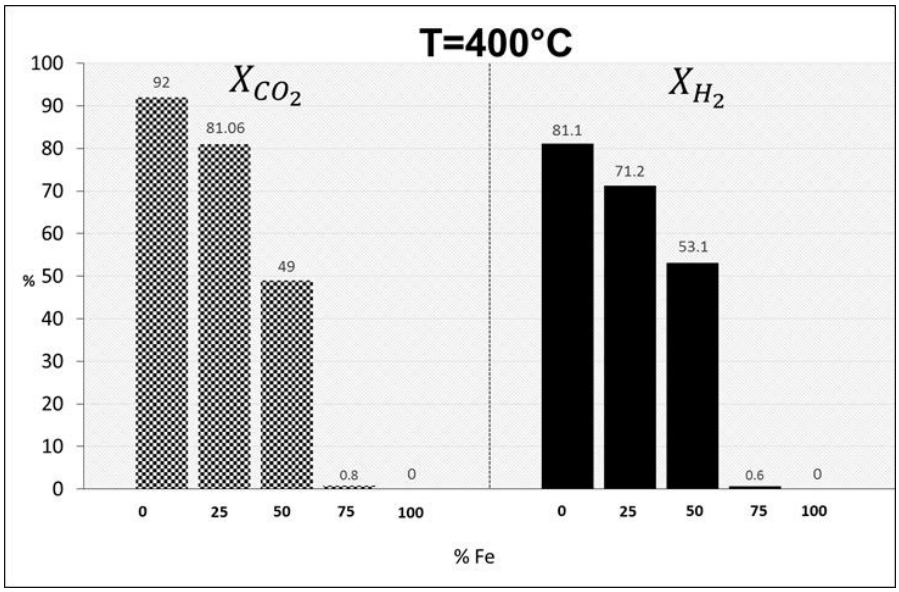
T=400°C
X_{CO_2}
X_{H_2}
%
92
81.06
49
0.8
0
81.1
71.2
53.1
0.6
0
0
25
50
75
100
% Fe

Figura 11

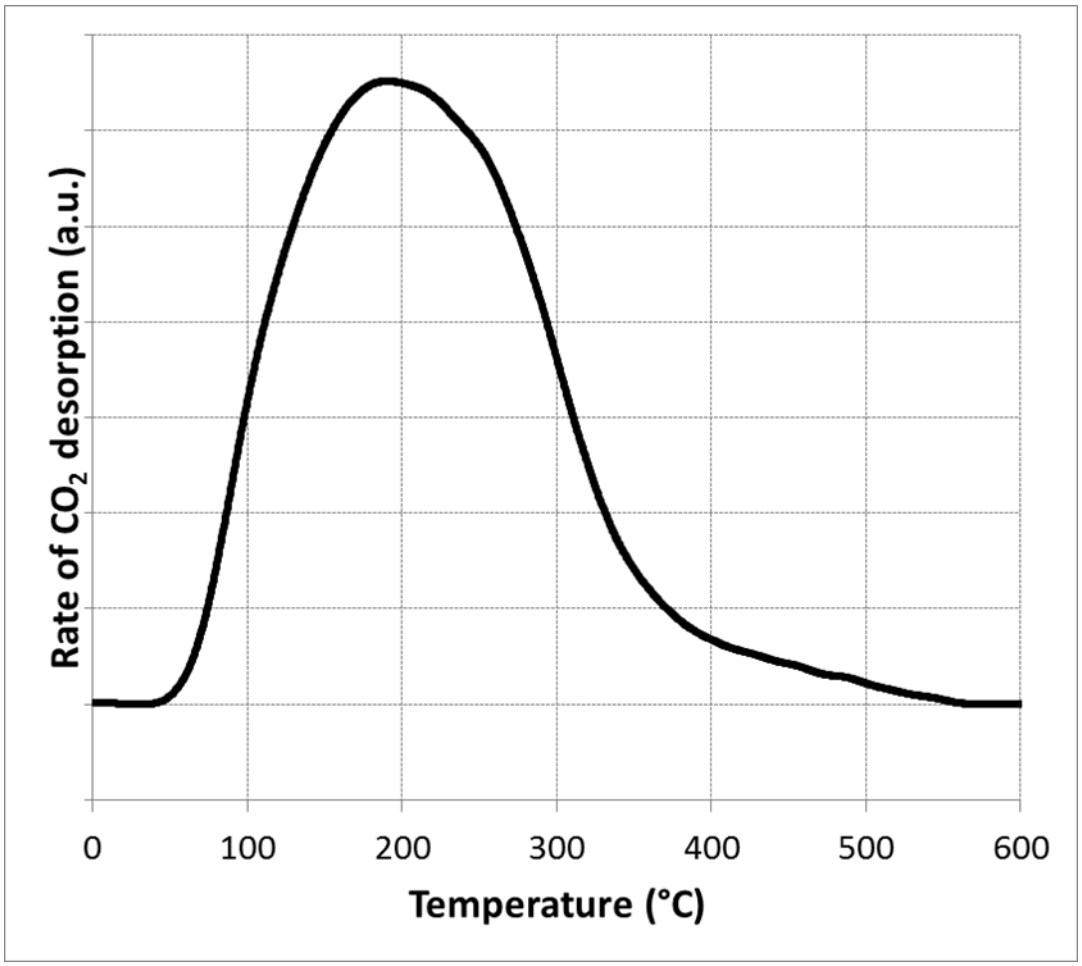

Sample	Tmax (°C)	CO2 uptake (micromol/g)
GDC	190	741

Figura 12